ACS Medicinal Chemistry Letters

pubs.acs.org/acsmedchemlett Letter

Designing Dihydrofolate Reductase Inhibitors as X-ray Radiosensitizers to Reverse Radioresistance of Cervical Cancer

Yuanwei Liang,[‖] Delong Zeng,[‖] Yuanyuan You, Bin Ma, Xiaoling Li, and Tianfeng Chen*

Cite This: *ACS Med. Chem. Lett.* 2020, 11, 1421−1428 Read Online

ACCESS | Metrics & More | Article Recommendations | Supporting Information

ABSTRACT: X-ray radiotherapy has been widely used in the treatment of cervical cancer, a common gynecologic malignant tumor. However, the therapeutic efficacy tends to be indistinctive. One major reason for this is amplification of the dihydrofolate reductase (DHFR) gene, which causes an increase in DHFR activity and attenuation of the treatment effect. To solve this problem, we synthesized a series of DHFR inhibitors derived from methotrexate (MTX) analogues as radiotherapy sensitizers. Activity screening revealed that compound **2a** exerted the best inhibitory effect toward DHFR activity. In combination with X-ray radiotherapy (4 Gy), **2a** showed much more prominent antiproliferative activity on cervical cancer cells than **2a** or X-rays alone and revealed higher selectivity and radiosensitization than MTX. In vitro experiments showed that **2a** + X-rays significantly induced cell apoptosis, as revealed by the increase in the Sub-G1 population and activation of caspase 3, 8, and 9. The in vivo antitumor effect demonstrated that in the presence of X-rays, **2a** effectively suppressed tumor growth and did not cause obvious side effects. In conclusion, as a DHFR inhibitor, **2a** successfully reversed the radioresistance problem induced by radiotherapy and greatly promoted the therapeutic effect. This is a promising candidate for tumor treatment that deserves further research and development. This study clearly demonstrates that DHFR inhibitors could be developed as promising radiosensitizers in the treatment of cervical cancer and that further research to improve their activity and potential in future clinical use is deserved.

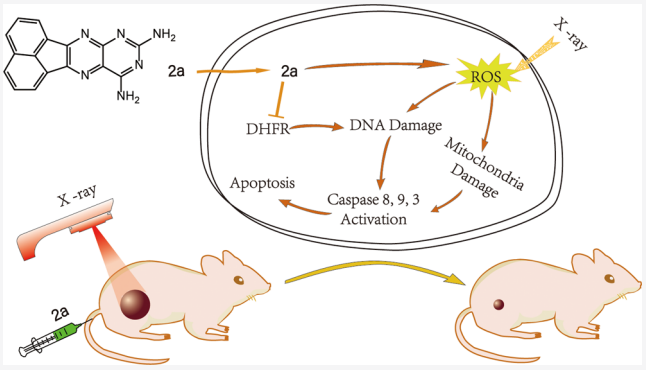

KEYWORDS: *DHFR inhibitor, radiotherapy, sensitizers, gene amplification*

Cervical cancer is a common cancer among female patients with genital diseases. Radiotherapy has become one of the most important treatments applied in all stages.[1] However, radiotherapy tends to trigger amplification of the dihydrofolate reductase (DHFR) gene,[2−4] which enhances the DHFR activity. DHFR is a critical enzyme for the synthesis of thymidine, which is the precursor of DNA. Enhancement of the DHFR activity promotes DNA replication of tumor cells, resulting in attenuation of the treatment effect. Thus, if the DHFR activity is inhibited, radiotherapy effects would be improved to varying degrees.[5,6]

Different types of tumor cells show different forms of response to ionizing radiation. For instance, lymphoma responds pretty well,[7] whereas HeLa cells are not sensitive to ionizing radiation.[8] One of the mechanisms of radiotherapy is that the hydrolytic dissociation by high-energy rays forms reactive oxygen species (ROS), which oxidize, attack, and damage DNA bases and cellular structure, resulting in tumor cell death.[9] The DNA replication and repair processes require a sufficient supply of bases. Once the synthesis of bases is impeded, DNA replication and repair are blocked.[10] DHFR inhibitors, such as methotrexate (MTX), mainly impede the synthesis of thymidine, leading to blocking of DNA synthesis. Thus, in the presence of X-rays, the use of MTX analogues as sensitizers is hopeful to improve the treatment efficacy because of their inhibitory effects toward DHFR.[11−14]

Deriving from the parent structure (2,4-diaminopteridine) of MTX, a series of 2,4-diaminopteridine analogues were synthesized as DHFR inhibitors in this work. Their structures are shown in Figure 1A, and their anticancer activities in the presence or absence of X-rays (4 Gy) were compared. In the screening of inhibitory activity toward DHFR, compound **2a** showed the highest activity among the synthetic compounds. Meanwhile, **2a**-induced cell death and ROS-mediated mitochondrial dysfunction in the presence of X-rays and the in vivo effects on HeLa cells were also investigated. This study clearly demonstrates that these synthetic DHFR inhibitors deserve further investigation as promising radiosensitizers in

Received: March 11, 2020
Accepted: June 17, 2020
Published: June 17, 2020

https://dx.doi.org/10.1021/acsmedchemlett.0c00105
ACS Med. Chem. Lett. 2020, 11, 1421−1428

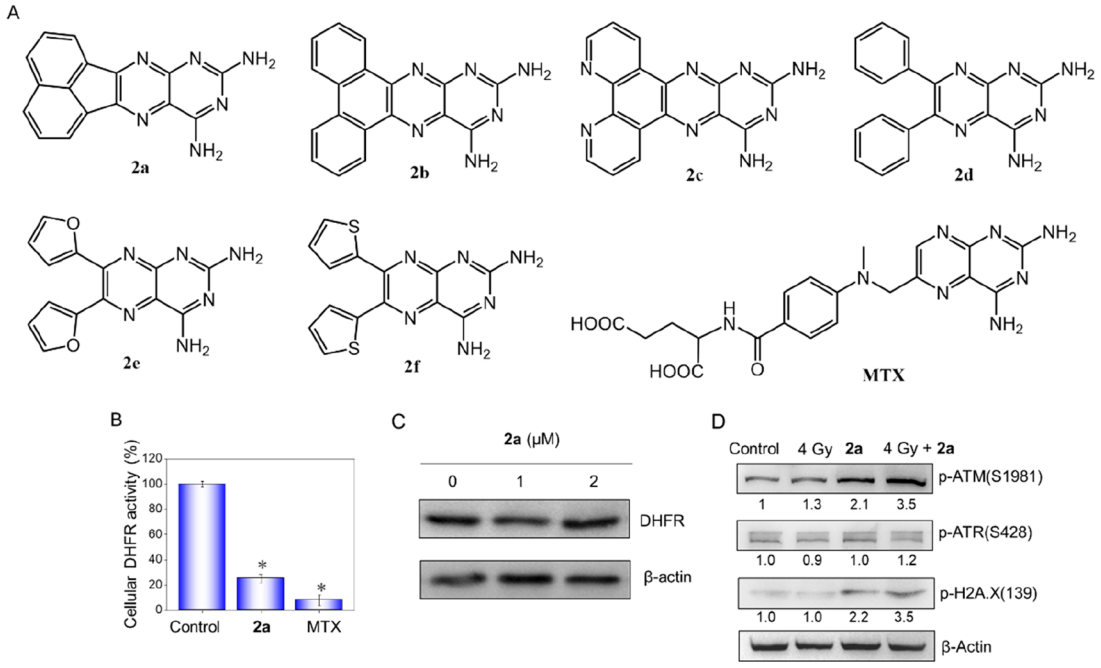

Figure 1. Structures of the synthetic 2,4-diaminopteridine derivatives and inhibitory effects of **2a** on intracellular DHFR activity and enhancement on X-ray-induced DNA damage. (A) Structures of the synthetic 2,4-diaminopteridine derivatives and MTX. (B) DHFR activities in lysates of HeLa cells treated with **2a** at a concentration of 2 μM. (C) Protein levels of DHFR from cell lysates analyzed by Western blotting. (D) Efficient activation of ATM and H2A.X by **2a** and X-rays after DNA replication stress. After treatment for 48 h, cells were harvested, lysed, and subjected to Western blotting.

Table 1. Cytotoxic Activities of 2,4-Diaminopteridine Derivatives on HeLa Cancer Cells and Ect1/E6E7 Normal Cells with (4 Gy) or without (0 Gy) X-rays by MTT Assay

	IC_{50} (μM)						
	2a	**2b**	**2c**	**2d**	**2e**	**2f**	MTX
HeLa + 0 Gy	2.1 ± 0.2	>80	9.8 ± 0.3	32.6 ± 1.2	24.5 ± 1.2	4.6 ± 0.3	1.5 ± 0.2
HeLa + 4 Gy	0.64 ± 0.03	>80	6.3 ± 0.2	14.8 ± 0.4	14.6 ± 0.8	2.3 ± 0.2	0.82 ± 0.08
SER[a]	3.3 ± 0.2	NA	1.6 ± 0.1	2.20 ± 0.2	1.7 ± 0.1	2.0 ± 0.4	1.8 ± 0.3
Ect1/E6E7 + 0 Gy	6.9 ± 0.3	>80	20.0 ± 1.0	59.3 ± 1.6	40.1 ± 1.6	10.9 ± 1.8	2.9 ± 0.3
Ect1/E6E7 + 4 Gy	3.1 ± 0.2	>80	13.9 ± 1.0	38.1 ± 1.9	19.8 ± 1.2	5.3 ± 0.3	1.8 ± 0.2
SER[b]	2.2 ± 0.1	NA	1.4 ± 0.2	1.6 ± 0.1	2.0 ± 0.1	2.1 ± 0.2	1.6 ± 0.3
SI_0[c]	3.3 ± 0.4	NA	2.0 ± 0.1	1.8 ± 0.1	1.6 ± 0.1	2.5 ± 0.3	1.9 ± 0.2
SI_4[d]	4.8 ± 0.5	NA	2.2 ± 0.1	2.6 ± 0.1	1.4 ± 0.1	2.3 ± 0.4	2.2 ± 0.1

[a]Sensitivity enhancement ratio (SER) = IC_{50}(HeLa + 0 Gy)/IC_{50}(HeLa + 4 Gy). [b]SER = IC_{50} (Ect1/E6E7 + 0 Gy)/IC_{50} (Ect1/E6E7 + 4 Gy). [c]Safe index for 0 Gy (SI_0) = (Ect1/E6E7 + 0 Gy)/(HeLa + 0 Gy). [d]Safe index for 4 Gy (SI_4) = (Ect1/E6E7 + 4 Gy)/(HeLa + 4 Gy).

clinical therapy for cervical cancer to improve their treatment efficacy.

Synthesis. Compounds **2a**–**f** (Figure 1A) were prepared according to Scheme S1. The general principle for the synthetic approach to 2,4-diaminopteridine derivatives was based on the condensation of pyrimidine-2,4,5,6-tetraamine with different substituted biacetyls in refluxing EtOH. Their structures were confirmed by NMR and MS analyses (Figures S1–S17).

In Vitro Antiproliferative Activities of 2,4-Diaminopteridine Derivatives in Combination with X-rays against HeLa Cells. The antiproliferative activities of the 2,4-diaminopteridine derivatives alone and in combination with X-rays (4 Gy) against HeLa cells were measured, and the results are shown in Figure S18. The IC_{50}'s of synthetic 2,4-diaminopteridine derivatives toward HeLa cancer cells and Ect1/E6E7 normal cells are shown in Table 1. In general, we identified MTX > **2a** > **2f** > **2c** > **2e** > **2d** > **2b** in terms of IC_{50}. Moreover, in combination with X-rays, the antiproliferative activities of all of the compounds except **2b** improved to varying degrees. It is worth noting that in the presence of X-rays, **2a** (0.64 μM) surpassed MTX (0.82 μM), with a sensitivity enhancement ratio (SER) of 3.3, which is larger than that of MTX (1.8).

On the other hand, the cytotoxic activities of the diaminopteridine derivatives against Ect1/E6E7, a normal ectocervix epithelial cell line, were also determined. The results displayed that MTX exhibits high toxicity toward Ect1/E6E7 cells with IC_{50}'s of 2.9 μM (+0 Gy) and 1.8 μM (+4Gy). However, the toxicity of **2a** against Ect1/E6E7 was lower than that of MTX, with IC_{50}'s of 6.9 and 3.1 μM, respectively. Similarly, the other diaminopteridines possessed a certain extent of selectivity, which were reflected by the safe indexes (SIs) with X-rays (4 Gy) (SI_4) or without X-rays (SI_0). Especially, the SI_4 of **2a** was 4.8, which was more than 2-fold larger compared with MTX. These results led to the

https://dx.doi.org/10.1021/acsmedchemlett.0c00105
ACS Med. Chem. Lett. 2020, 11, 1421–1428

conclusion that **2a** demonstrated apparent sensitization in the presence of X-rays (4 Gy) against HeLa cell lines and possessed a certain extent of selectivity.

Evaluation of In Vitro DHFR Inhibitory Activities of 2a−f. After investigating the cytotoxic activities of 2,4-diaminopteridine derivatives, we next wanted to determine whether there were similar discrepancies in the inhibitory effects of **2a−f** on DHFR activity. The DHFR inhibitory activities of **2a−f** along with MTX as a comparison were determined using a DHFR assay kit (Sigma-Aldrich, S0340); the results are presented in Figure S19, and the IC_{50} values are presented in Table 2. Although **2a**, **2b**, and **2c** possess a similar planar structure, they showed significantly different inhibitory activities against DHFR. **2a** exhibited the best inhibitory efficacy among the six compounds, with an IC_{50} of 0.81 μM, followed by **2f** (IC_{50} = 1.43 μM). **2c** had moderate inhibitory activity, with an IC_{50} of 5.8 μM. It can thus be seen that the inhibitory activities of **2a**, **2f**, and **2c** corresponded well with their antiproliferative activities. On the other hand, **2b**, with a similar planar structure as **2a**, exhibited the worst activity, with IC_{50} > 50 μM. Besides, **2d** and **2e** had similar structures with rotatable substituent groups at the 6- and 7-position and showed relatively poor activities against DHFR, with IC_{50}'s of 13.6 and 10.4 μM, respectively. Together, our results showed that **2a** has the most excellent inhibitory activity against DHFR among the six compounds.

Table 2. IC_{50} Values for Inhibition of DHFR Activity by Compounds 2a−f

compound	IC_{50} (μM)
2a	0.81 ± 0.10
2b	>50
2c	5.8 ± 0.36
2d	13.6 ± 0.59
2e	10.4 ± 0.44
2f	1.43 ± 0.19
MTX	0.083 ± 0.005

2a Inhibits DHFR Activity and Activates ATM and H2A.X in Response to DNA Replication Stress. As the leading drug, **2a** was used to evaluate the inhibitory effects on intracellular DHFR on account of its best inhibitory effect against DHFR in vitro among the six synthetic derivatives. Meanwhile, MTX was used as a positive control. The results showed that intracellular DHFR activity was obviously inhibited by **2a** at the cytotoxic concentrations of 10 μM (76% inhibition compared with the control) (Figure 1B). However, a more apparent inhibitory effect on DFHR can be seen for MTX (91% inhibition). This corresponded well with the IC_{50} values against HeLa cells. Therefore, the prominent antiproliferative activity of **2a** was mainly attributed to the inhibitory effect on DHFR. Western blot analyses (Figure 1C) indicated that there was obvious change in protein levels of DHFR in cells treated with **2a**, demonstrating that the decline of intracellular DHFR activity was regulated by **2a** and not associated with downregulation of DHFR protein levels.

DHFR is indispensable for the synthesis of nucleic acids. Therefore, the inhibition of DHFR activity gives rise to DNA replication stress. Persistent replication stress results in phosphorylation of DNA-damage-dependent kinases such as ATR, ATM, and DNA-PK. Western blotting results (Figure 1D) showed that no distinct phosphorylation of ATR can be seen in the treatment groups compared with the control group. However, an obvious increase in ATM phosphorylation following treatment with **2a** or X-rays alone can be observed. Meanwhile, the phosphorylation level of ATM increased much more significantly in the **2a** + X-rays group than in the groups with **2a** or X-rays alone. Furthermore, we also examined the level of γ-H2A.X, which is the phosphorylated form of H2A.X produced by ATR, ATM, and DNA-PK. Meanwhile, γ-H2A.X is essential for checkpoint-related cell-cycle arrest and DNA repair resulting from ionizing radiation or chemotherapeutic agent, which leads to rapid phosphorylation of H2A.X at Ser139. Our results showed that X-rays alone did not cause

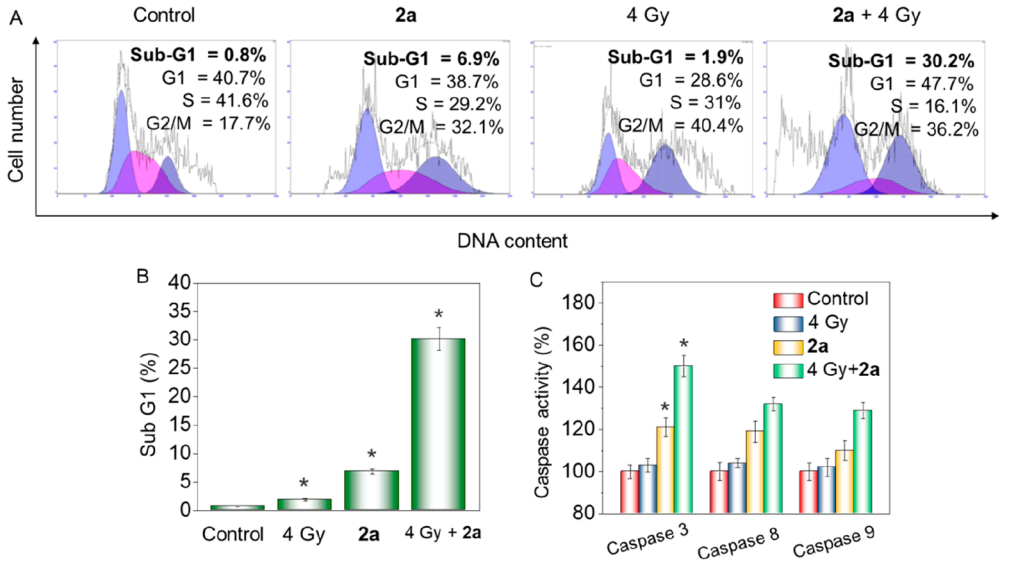

Figure 2. 2a combines with X-rays to promote apoptosis of HeLa cells. (A) Flow cytometry analysis indicated the distribution of cell cycle in HeLa cells. Cells were treated with **2a** (1 μM) without or with X-rays (4 Gy) for 48 h. (B) Percentages of Sub-G1 phase population. (C) Activities of caspase 8, 9, and 3 on HeLa cells after treatment with **2a** (1 μM) without or with X-rays (4 Gy) for 12 h. Values are shown as mean ± SD for three independent experiments. Bars are statistically different at $^*p < 0.05$.

https://dx.doi.org/10.1021/acsmedchemlett.0c00105
ACS Med. Chem. Lett. 2020, 11, 1421−1428

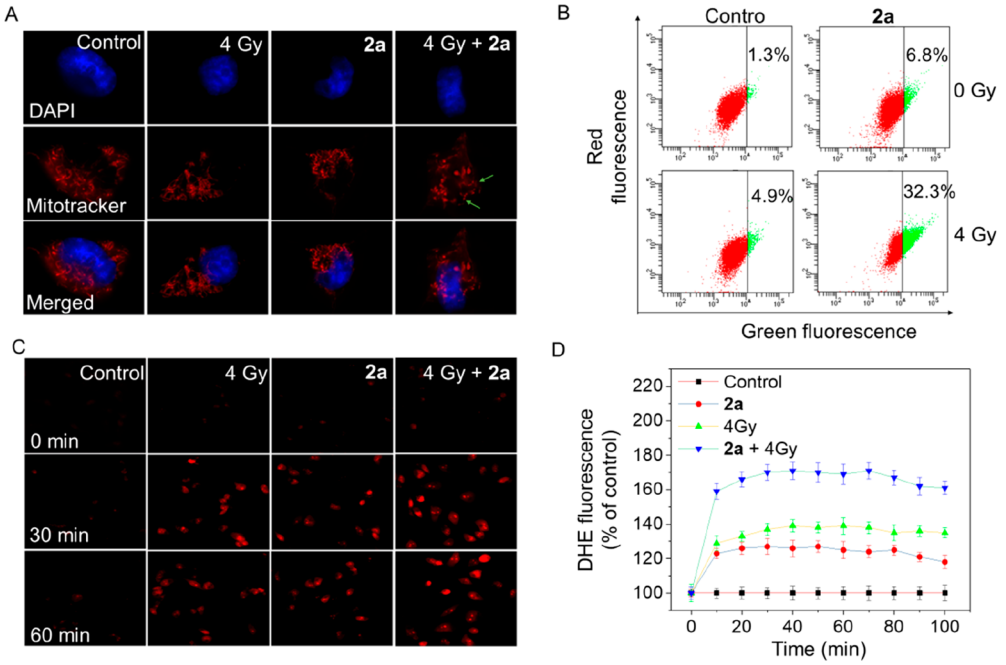

Figure 3. Synergistic effect of **2a** and X-rays on induction of mitochondrial dysfunction and ROS generation. (A) Fluorescent micrographs of mitochondrial fission induced by **2a** (1 μM) in the absence or presence of X-rays (4 Gy). The photomicrographs were detected using Mitotracker and DAPI costaining. (B) Flow cytometry analysis of the changes in $\Delta\Psi$m on HeLa cells treated with **2a** (1 μM) without or with X-ray treatment. (C) Fluorescence images of intracellular ROS detected by DHE probe on HeLa cells. (D) Fluorescence microplate readings for intracellular ROS measured by DHE probe on HeLa cells.

H2A.X phosphorylation but that **2a** alone or combined with X-rays resulted in distinct phosphorylation of γ-H2A.X. This demonstrates that phosphorylation of ATM and H2A.X plays a critical role in the response of **2a**-induced DNA replication stress.

2a Combines with X-rays to Promote Apoptosis of HeLa Cells. Anticancer drugs typically exert their cytotoxic effects by triggering cell-cycle arrest or apoptosis in susceptible cells.[15,16] To understand the mechanism of drug action induced by **2a** in the absence or presence of X-rays, cell-cycle assays were performed. Figure 2A shows that X-rays alone caused apparent G2/M phase arrest in HeLa cells from 17.7% (control) to 40.4%. Besides, cells treated with **2a** showed a moderate level of G2/M arrest accompanied by a rise in the Sub-G1 peak, accounting for 6.9%, demonstrating that apoptosis is involved in **2a**-triggered cell death. Interestingly, cells treated with **2a** and X-rays together exerted a remarkable synergistic effect, as the Sub-G1 peak shot up to 30.2% (Figure 2B), indicating a marked increase of apoptosis. These data showed that apoptosis was mainly involved in the synergistic action of **2a** and X-rays on HeLa cells.

The caspase cascade system is closely related to the intracellular apoptosis signals, such as signal induction, transduction, and amplification.[17,18] Since apoptosis-inducing effects and anticancer activity of X-rays were significantly amplified by **2a**, detection of caspase activity was subsequently conducted. As shown in Figure 2C, the activation of caspase 8, 9, and 3 by X-rays alone was limited, whereas they were effectively activated to various degrees by **2a** (caspase 3 > caspase 8 > caspase 9). Moreover, the activation was apparently improved by the addition of **2a** to X-rays, and the improvement was more distinct for caspase 3 and 8, from 121% to 150% and 110% to 129%, respectively. These data demonstrated that **2a** was able to activate caspase 8 and caspase 9, which gave rise to the activation of executor caspase 3 and resulted in apoptosis. The activation was apparently improved and apoptosis was obviously promoted when **2a** was used in combination with X-rays.

Synergistic Effect of 2a and X-rays Improved Mitochondrial Dysfunction and ROS Generation. Mitochondrial dysfunction has been demonstrated to be closely related to cellular apoptosis and plays a vitally important in the apoptotic pathway.[19,20] Mitochondria are typically strewn through the whole cytoplasm, and the structures are mostly long, tubular, or filamentous. Mitochondrial fission has vital implications in stress response and apoptosis. Herein, the change in mitochondrial morphology was also studied. As shown in Figure 3A, treatment of cells with X-rays or **2a** alone gave rise to slight mitochondrial fission. Moreover, the fission became significantly apparent when cells were treated with the combination of **2a** and X-rays (4 Gy).

The loss of mitochondrial membrane potential (MMP) has been proved to be an early event during the apoptotic process.[21] To evaluate the role of the MMP in **2a**-treated cells, the status of $\Delta\Psi$m was studied by JC-1 flow cytometric analysis (Figure 3B). Our results indicated that cells treated with **2a** (1 μM) or X-rays (4 Gy) alone displayed only limited depletion of $\Delta\Psi$m (6.8% and 4.9%, respectively; the green fluorescence represents the proportion of loss of $\Delta\Psi$m). However, the combination of **2a** and X-rays induced a significant rise in the proportion of depolarized mitochondria (up to 32.3%), demonstrating that in the presence of X-rays, a low **2a** concentration gave rise to rapid dissipation of $\Delta\Psi$m compared with **2a** alone. These data showed that mitochondrial dysfunction contributed to **2a**-induced apoptosis on HeLa cells and that the dysfunction was apparently amplified in the presence of X-rays.

https://dx.doi.org/10.1021/acsmedchemlett.0c00105
ACS Med. Chem. Lett. 2020, 11, 1421−1428

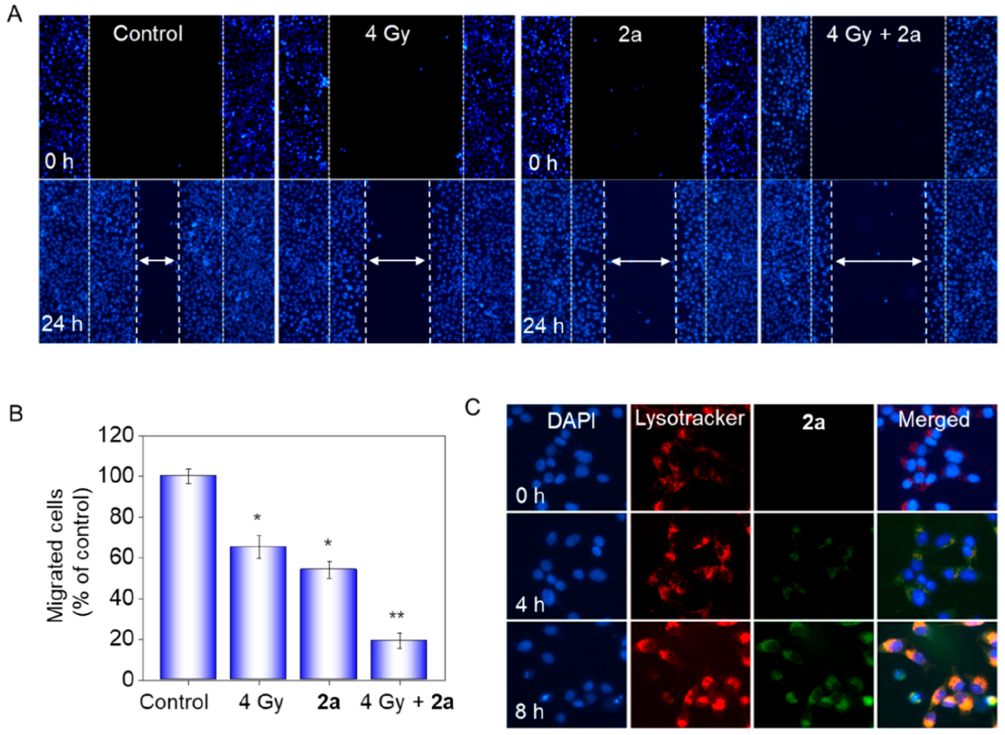

Figure 4. Synergistic inhibition of migration by **2a** and X-rays and cellular localization of **2a** in HeLa cells. (A) Cancer cell migration was inhibited by treatment with **2a** in the absence or presence of X-rays (4 Gy). Wound closure was recorded under phase-contrast microscopy at the indicated times. (B) Quantitative analysis of the migrated cells by manual counting. Values are expressed as mean ± SD of three independent experiments. (C) Intracellular trafficking of **2a** in individual HeLa cells. The cells were pretreated with **2a** (20 μM) in a 2 cm dish and then stained with LysoTracker 2 h before the point in time and DAPI 30 min before the point in time, and then the fluorescence was captured under a fluorescence microscope.

Reactive oxygen species (ROS) is a collective term for various oxygen-containing reactive and short-lived molecules.[22] Ionizing radiation has been shown to typically generate ROS in a variety of cell types.[23] ROS-induced oxidative injury causes DNA damage (mutations), protein oxidation, and lipid peroxidation. Under the circumstance of redox imbalance, cells react rapidly to give a plethora of biological responses. Rapid responses include cell-cycle-specific growth arrest, gene transcription, activation of signaling pathways, and repair of damaged DNA, which determine cell fates such as necroses, senesce, apoptosis, and proliferation. Therefore, we investigated ROS generation in HeLa cells by the use of the fluorescent probe dihydroethidium (DHE). Chemically reduced and acetylated forms of DHE are nonfluorescent. Upon reaction with superoxide anions, DHE forms a red fluorescent product (2-hydroxyethidium). Oxidation of these probes can be detected by monitoring the increase in fluorescence using a microplate reader or fluorescence microscope.

The fluorescence microscopy results (Figure 3C) showed that HeLa cells pretreated with X-rays (4 Gy) or **2a** alone and then incubated with DHE for 30 min turned red, demonstrating the generation of a certain level of ROS. This fluorescence still remained in the next 30 min. Notably, the brightness of the DHE probe became higher when cells were treated with **2a** and X-rays (4 Gy) together at the same time point. Meanwhile, microplate reader results (Figure 3D) showed that exposing HeLa cells to X-rays (4 Gy) alone triggered a 150% increase of ROS generation compared with nonirradiated cells. Treatment with **2a** alone caused only a 132% increase in ROS. Interestingly, the ROS level of **2a**-treated cells increased significantly in the presence of X-rays, rising to 205%. These results revealed that the synergistic effect of X-rays and **2a** in inducing extensive accumulation of ROS is important and mediates the apoptosis of HeLa cells.

2a and X-rays Synergistically Inhibit the Migration of HeLa Cells. On many occasions, tumor metastasis is the major cause of higher death rates.[24] Tumor cells tend to spread from the original site to adjacent sites and form secondary tumors. Metastasis occurs via immigration and infiltration of the original tumor to distant organs and tissue. For most clinical drugs, prevention of metastatic diseases becomes rather important beyond killing the tumor cells in the therapeutic process. Thus, a wound-healing migration assay was performed on HeLa cells. Figure 4A shows that the average cell migration velocity was reduced by X-rays or **2a** alone (**2a** > X-rays) in comparison with the control, indicating that the ability of cell movement was suppressed. Notably, combination treatment of **2a** and X-rays resulted in a significant decrease in the spreading rate. The level of cell migration into the wound scratch was quantified and is shown in Figure 4B. To be specific, X-rays and **2a** alone suppressed 35% and 46% of migration of HeLa cells, respectively. The migration was suppressed up to 81% when cells were treated with X-rays and **2a** together.

On the basis of the fluorescence spectrum of **2a**, in which the maximum emission wavelength is about 510 nm, the fluorescence color should be green. To further confirm intracellular localization, DAPI and LysoTracker (red) were used to stain the nucleus and lysosomes, respectively. As shown in Figure 4C, after incubation of **2a** for 4 h, the green fluorescence of **2a** was well-overlapped with the red fluorescence, whereas this overlap was not so apparent in the

https://dx.doi.org/10.1021/acsmedchemlett.0c00105
ACS Med. Chem. Lett. 2020, 11, 1421−1428

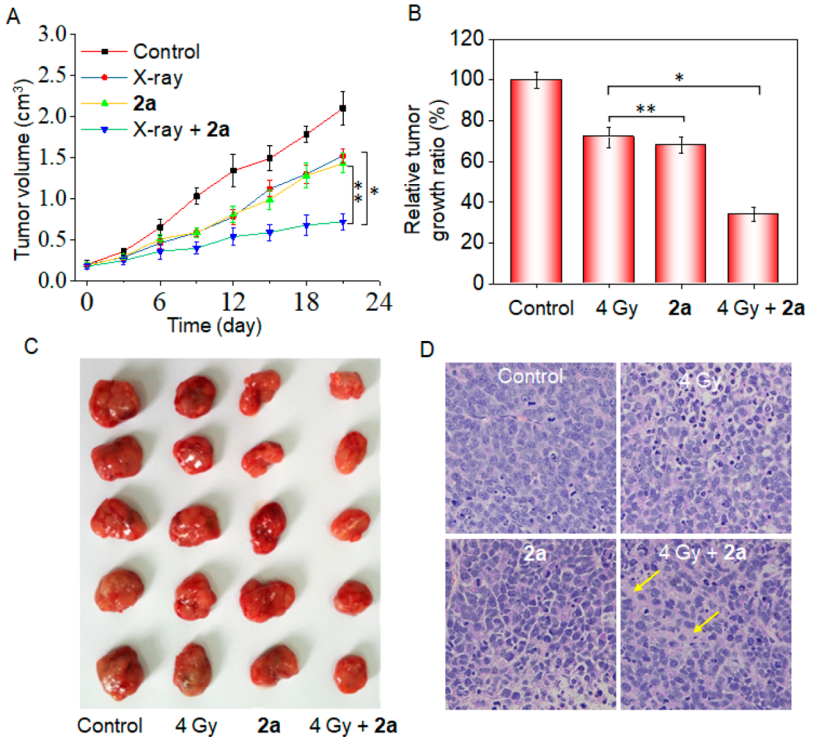

Figure 5. In vivo anticancer activity of **2a** and X-rays. (A) Changes in tumor volume of **2a**-treated HeLa xenografts on nude mice in the presence or absence of X-rays. (B) Relative tumor growth rates. (C) Tumor photographs collected from different groups. (D) H&E staining in tumor tissue sections from different groups of mice.

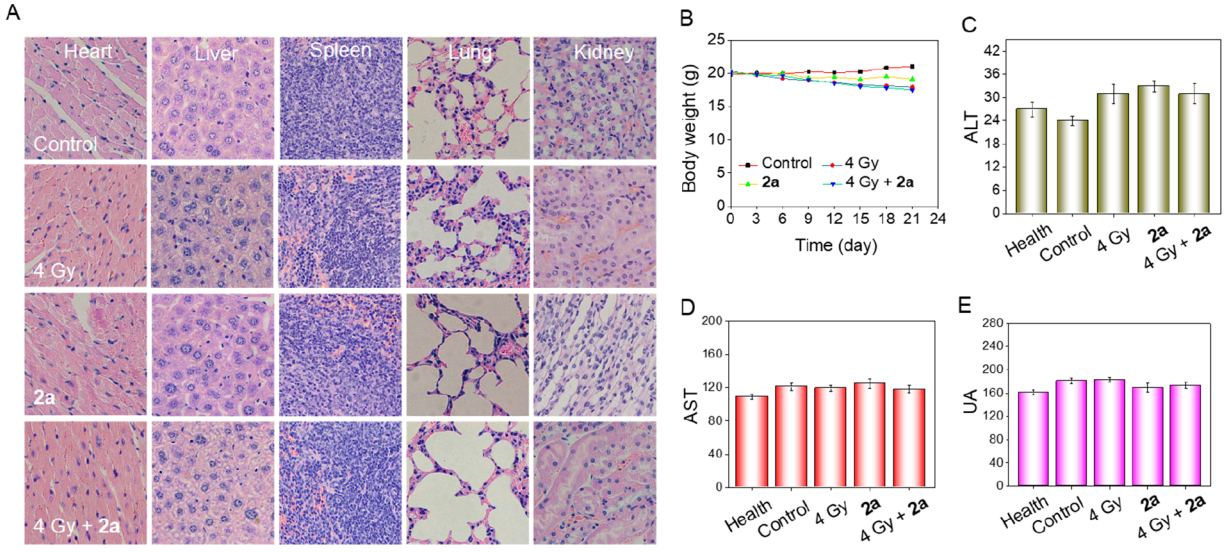

Figure 6. Acute toxicity evaluation of **2a**. (A) H&E staining sections of main organs from nude mice after treatment with **2a** in the absence or presence of X-rays. (B) Record of the body weight over 21 days. (C–E) Blood biochemistry analyses of ALT (C), AST (D), and UA (E) in mice after different treatments.

next 4 h, demonstrating that **2a** accumulated in lysosomes at first and then diffused into the cytoplasm.

In Vivo Anticancer Activity of 2a and in Combination with X-rays. The therapeutic efficacy of compound **2a** in the absence or presence of X-rays was also measured in HeLa-tumor-bearing nude mice. Nude mice bearing HeLa tumors were treated with **2a** through tail intravenous injection every 3 days during the 21-day period at a dose of 4 mg/kg. As shown in Figure 5A, X-rays exerted a certain degree of inhibitory effect on tumor growth, as demonstrated by the decreased growth in tumor volume in comparison with the control group (Figure 5B). **2a**, which had obvious antiproliferative activity compared with X-rays in vitro, exerted similar inhibitory effects on tumor growth throughout the 21-day period. It is worth noting that when **2a** was combined with X-rays, their inhibitory effect on tumor growth was significantly improved, as the relative tumor growth ratio decreased to 32%. This was confirmed by the tumor photographs from different groups (Figure 5C). In addition, histological section analysis (Figure 5D) also displayed that the combination treatment induced

https://dx.doi.org/10.1021/acsmedchemlett.0c00105
ACS Med. Chem. Lett. 2020, 11, 1421−1428

much more remarkable tumor destruction than X-rays or **2a** alone. These data indicated that in combination with X-rays, **2a** significantly inhibited tumor growth.

In Vivo Toxicity of 2a. Folic acid analogues such as methotrexate and trimethoprem typically have potential hepatotoxicity (fatty liver disease and even cirrhosis), renal toxicity, and neurovirulence.[25] To evaluate the systemic toxicities of compound **2a** in vivo, mice were euthanized 24 h after the last injection. Hematoxylin and eosin (H&E) staining was conducted on major organs, and the blood was collected for biochemistry analysis. The results showed that the heart, liver, lungs, kidneys, and spleen all witnessed no evident damage after irradiation with X-rays or treatment of **2a** (4 mg/kg), as reflected by the observation that X-ray-irradiated or **2a**-treated mice did not show a significant difference with control group (Figure 6A). Meanwhile, the synergistic effect of X-rays and **2a** together also showed no apparent damage to these organs.

Drug toxicity typically brings about a variation in body weight (mostly weight loss). Figure 6B shows the records of body weight throughout the treatment period between the first day and the 21st day. In the control group, there was a slight increase in body weight after 21 days of treatment, and there was not much change in **2a**-treated mice. X-rays, with similar tumor inhibitory rate compared with **2a**, resulted in moderate weight loss. However, in the presence of X-rays, the therapeutic effect **of 2a** was greatly improved but did not bring about further apparent weight loss compared with X-rays alone.

Furthermore, blood biochemistry analysis, including liver function indicators (alanine aminotransferase (ALT) and aspartate aminotransferase (ALT)) and kidney function indicators (blood urea nitrogen (BUN) and uric acid (UA)) showed that **2a**-treated or X-ray-irradiated nude mice as well as mice that received the combination treatment of X-rays and **2a** did not exhibit acute or further adverse effects in the liver and kidney, indicating that the therapy did not mess up the normal function of the liver (Figure 6C,D) and kidneys (Figures 6E and S20). This was different from most classical folic acid analogues, which typically induce different levels of liver and kidney toxicity.[26] Even in combination with X-rays, **2a** posed no apparent side effects on nude mice. These data indicated the remarkable tumoricidal efficacy and limited side effects of compound **2a** in the presence of X-rays and its clinical potential and promising application prospects.

We next investigated the cellular uptake of **2a** and MTX. The results showed that the cellular uptake rate of **2a** was much higher than that of MTX (Figure S21), indicating that the increased antiproliferative effects could be due to the increased cellular uptake rate.

Furthermore, the pharmacokinetic parameters, including elimination-phase half-life period of medicine ($t_{1/2}\beta$), area under the concentration versus time curve from 0 to 48 h (AUC_{0-48h}), maximum concentration observed (C_{max}), clearance of medicine (Cl), and mean retention time (MRT) were also tested. These results demonstrated the moderate blood circulation of **2a**.

Conclusions. Amplification of the DHFR gene may make radiotherapy for cervical cancer indistinctive. As a consequence, the increase in DHFR activity causes attenuation of the treatment effect. In this study, we synthesized a series of DHFR inhibitors derived from methotrexate analogues as radiotherapy sensitizers to reverse the radiotherapy resistance in cervical cancer. Our results revealed the following: (i) among the compounds synthesized, the leading compound **2a** exerted the best inhibitory effects toward the activity of DHFR; (ii) the combination of **2a** and X-ray radiotherapy exerted much stronger effects in killing cervical cancer cells than **2a** or X-rays alone, with higher selectivity and radiosensitization activity than MTX; (iii) the combination of X-rays and **2a** effectively caused cell death by triggering cell apoptosis through activation of caspase 8, 9, and 3 and ROS-mediated mitochondria dysfunction; (iv) in combination with X-rays, **2a** notably suppressed the migration capacity of HeLa cells; and (v) in the presence of X-rays, **2a** effectively suppressed tumor growth and did not cause obvious side effects in vivo. In conclusion, as a DHFR inhibitor, **2a** successfully reversed the radioresistance of cervical cancer cells and greatly promoted the therapeutic effect. The combination of the DHFR inhibitor and radiotherapy proved to be a promising strategy in cervical cancer therapy.

■ ASSOCIATED CONTENT

Supporting Information

The Supporting Information is available free of charge at https://pubs.acs.org/doi/10.1021/acsmedchemlett.0c00105.

Synthetic experimental details, related spectroscopic data for the compounds, and biological assay protocols (PDF)

■ AUTHOR INFORMATION

Corresponding Author

Tianfeng Chen − *The First Affiliated Hospital and Department of Chemistry, Jinan University, Guangzhou 510632, China;* orcid.org/0000-0001-6953-1342; Email: tchentf@jnu.edu.cn

Authors

Yuanwei Liang − *The First Affiliated Hospital and Department of Chemistry, Jinan University, Guangzhou 510632, China*

Delong Zeng − *The First Affiliated Hospital and Department of Chemistry, Jinan University, Guangzhou 510632, China*

Yuanyuan You − *The First Affiliated Hospital and Department of Chemistry, Jinan University, Guangzhou 510632, China; Shenzhen Agricultural Product Quality and Safety Inspection and Testing Center (Guangdong Provincial Key Laboratory of Supervision and Administration of Edible Agricultural Products, Market Supervision Administration), Shenzhen, China*

Bin Ma − *The First Affiliated Hospital and Department of Chemistry, Jinan University, Guangzhou 510632, China*

Xiaoling Li − *The First Affiliated Hospital and Department of Chemistry and Institute of Food Safety and Nutrition, Jinan University, Guangzhou 510632, China*

Complete contact information is available at: https://pubs.acs.org/10.1021/acsmedchemlett.0c00105

Author Contributions

‖Y.L. and D.Z. contributed equally to this work.

Notes

The authors declare no competing financial interest.

■ ACKNOWLEDGMENTS

This work was supported by National Natural Science Foundation of China (21877049), the Major Program for Tackling Key Problems of Industrial Technology in

Guangzhou (201902020013), the Dedicated Fund for Promoting High-Quality Marine Economic Development in Guangdong Province (GDOE-2019-A31), the Guangzhou Key Laboratory of Molecular and Functional Imaging for Clinical Translation (Project 201905010003), the Science and Technology Program of Guangzhou (202002030170), and the Guangdong Natural Science Foundation (2017A030310409).

■ ABBREVIATIONS

DHFR, dihydrofolate reductase; ROS, reactive oxygen species; DHE, dihydroethidium; MTX, methotrexate; ALT, alanine aminotransferase; AST, aspartate aminotransferase; UA, uric acid; BUN, blood urea nitrogen; $t_{1/2}\beta$, elimination phase, half-life period of medicine; AUC_{0-48h}, area under the concentration versus time curve from 0 to 48 h; C_{max}, maximum concentration observed; Cl, clearance of medicine; MRT, mean retention time

■ REFERENCES

(1) Moelle, U.; Mathewos, A.; Aynalem, A.; Wondemagegnehu, T.; Yonas, B.; Begoihn, M.; Addissie, A.; Unverzagt, S.; Jemal, A.; Thomssen, C.; Vordermark, D.; Kantelhardt, E. J. Cervical Cancer in Ethiopia: The Effect of Adherence to Radiotherapy on Survival. *Oncologist* **2018**, *23* (9), 1024−1032.

(2) Condit, P. T.; Ridings, G. R.; Coin, J. W.; Williams, G. R.; Mitchell, D., Jr.; Boles, G. W. Methotrexate and radiation in the treatment of patients with cancer. *Cancer Res.* **1964**, *24*, 1524−1533.

(3) Lustig, R. A.; DeMare, P. A.; Kramer, S. Adjuvant methotrexate in the radiotherapeutic management of advanced tumors of the head and neck. *Cancer* **1976**, *37* (6), 2703−2708.

(4) Hahn, P.; Nevaldine, B.; Morgan, W. F. X-ray induction of methotrexate resistance due to dhfr gene amplification, Somat. *Somatic Cell Mol. Genet.* **1990**, *16* (5), 413−423.

(5) Gresty, K. J.; Gray, K.-A.; Bobogare, A.; Wini, L.; Taleo, G.; Hii, J.; Cheng, Q.; Waters, N. C. Genetic mutations in Plasmodium falciparum and Plasmodium vivax dihydrofolate reductase (DHFR) and dihydropteroate synthase (DHPS) in Vanuatu and Solomon Islands prior to the introduction of artemisinin combination therapy. *Malar. J.* **2014**, *13*, 402.

(6) Francesconi, V.; Giovannini, L.; Santucci, M.; Cichero, E.; Costi, M. P.; Naesens, L.; Giordanetto, F.; Tonelli, M. Synthesis, biological evaluation and molecular modeling of novel azaspiro dihydrotriazines as influenza virus inhibitors targeting the host factor dihydrofolate reductase (DHFR). *Eur. J. Med. Chem.* **2018**, *155*, 229−243.

(7) Edeline, V.; Remouchamps, V.; Isnardi, V.; Vander Borght, T. Multimodality imaging using PET/CT ((18)F)-fluorodeoxyglucose for radiotherapy field delineation of localized Hodgkin lymphoma. *Cancer Radiother* **2018**, *22* (5), 384−392.

(8) Shi, D.; Liang, Z.; Zhang, C.; Zhang, H.; Liu, X. The effect of surgery on the survival status of patients with locally advanced cervical cancer after radiotherapy/chemoradiotherapy: a meta-analysis. *BMC Cancer* **2018**, *18* (1), 308.

(9) Yang, B.; Chen, Y.; Shi, J. Reactive Oxygen Species (ROS)-Based Nanomedicine. *Chem. Rev.* **2019**, *119* (8), 4881−4985.

(10) Trucco, L. D.; Mundra, P. A.; Hogan, K.; Garcia-Martinez, P.; Viros, A.; Mandal, A. K.; Macagno, N.; Gaudy-Marqueste, C.; Allan, D.; Baenke, F.; Cook, M.; McManus, C.; Sanchez-Laorden, B.; Dhomen, N.; Marais, R. Ultraviolet radiation-induced DNA damage is prognostic for outcome in melanoma. *Nat. Med.* **2019**, *25* (2), 221−224.

(11) Ng, H. L.; Ma, X.; Chew, E. H.; Chui, W. K. Design, Synthesis, and Biological Evaluation of Coupled Bioactive Scaffolds as Potential Anticancer Agents for Dual Targeting of Dihydrofolate Reductase and Thioredoxin Reductase. *J. Med. Chem.* **2017**, *60* (5), 1734−1745.

(12) Cammarata, M.; Thyer, R.; Lombardo, M.; Anderson, A.; Wright, D.; Ellington, A.; Brodbelt, J. S. Characterization of trimethoprim resistant E. coli dihydrofolate reductase mutants by mass spectrometry and inhibition by propargyl-linked antifolates. *Chem. Sci.* **2017**, *8* (5), 4062−4072.

(13) Loveridge, E. J.; Behiry, E. M.; Guo, J.; Allemann, R. K. Evidence that a 'dynamic knockout' in Escherichia coli dihydrofolate reductase does not affect the chemical step of catalysis. *Nat. Chem.* **2012**, *4* (4), 292−7.

(14) Burns, D. D.; Teppang, K. L.; Lee, R. W.; Lokensgard, M. E.; Purse, B. W. Fluorescence Turn-On Sensing of DNA Duplex Formation by a Tricyclic Cytidine Analogue. *J. Am. Chem. Soc.* **2017**, *139* (4), 1372−1375.

(15) Madungwe, N. B.; Feng, Y.; Lie, M.; Tombo, N.; Liu, L.; Kaya, F.; Bopassa, J. C. Mitochondrial inner membrane protein (mitofilin) knockdown induces cell death by apoptosis via an AIF-PARP-dependent mechanism and cell cycle arrest. *Am. J. Physiol Cell Physiol* **2018**, *315* (1), C28−C43.

(16) Liu, H.; Lin, W.; He, L.; Chen, T. Radiosensitive core/satellite ternary heteronanostructure for multimodal imaging-guided synergistic cancer radiotherapy. *Biomaterials* **2020**, *226*, 119545.

(17) Sallmyr, A.; Matsumoto, Y.; Roginskaya, V.; Van Houten, B.; Tomkinson, A. E. Inhibiting Mitochondrial DNA Ligase IIIalpha Activates Caspase 1-Dependent Apoptosis in Cancer Cells. *Cancer Res.* **2016**, *76* (18), 5431−41.

(18) He, L.; Huang, G.; Liu, H.; Sang, C.; Liu, X.; Chen, T. Highly bioactive zeolitic imidazolate framework-8-capped nanotherapeutics for efficient reversal of reperfusion-induced injury in ischemic stroke. *Science Advances* **2020**, *6*, No. eaay9751.

(19) Dai, C.; Ciccotosto, G. D.; Cappai, R.; Wang, Y.; Tang, S.; Hoyer, D.; Schneider, E. K.; Velkov, T.; Xiao, X. Rapamycin Confers Neuroprotection against Colistin-Induced Oxidative Stress, Mitochondria Dysfunction, and Apoptosis through the Activation of Autophagy and mTOR/Akt/CREB Signaling Pathways. *ACS Chem. Neurosci.* **2018**, *9* (4), 824−837.

(20) Huang, Y.; Fu, Y.; Li, M.; Jiang, D.; Kutyreff, C. J.; Engle, J. W.; Lan, X.; Cai, W.; Chen, T. Chirality-Driven Transportation and Oxidation Prevention by Chiral Selenium Nanoparticles. *Angew. Chem., Int. Ed.* **2020**, *59*, 4406−4414.

(21) Lee, D. G.; Choi, B. K.; Kim, Y. H.; Oh, H. S.; Park, S. H.; Bae, Y. S.; Kwon, B. S. The repopulating cancer cells in melanoma are characterized by increased mitochondrial membrane potential. *Cancer Lett.* **2016**, *382* (2), 186−194.

(22) Yang, W.; Tao, Y.; Wu, Y.; Zhao, X.; Ye, W.; Zhao, D.; Fu, L.; Tian, C.; Yang, J.; He, F.; Tang, L. Neutrophils promote the development of reparative macrophages mediated by ROS to orchestrate liver repair. *Nat. Commun.* **2019**, *10* (1), 1076.

(23) Park, M. T.; Kim, M. J.; Kang, Y. H.; Choi, S. Y.; Lee, J. H.; Choi, J. A.; Kang, C. M.; Cho, C. K.; Kang, S.; Bae, S.; Lee, Y. S.; Chung, H. Y.; Lee, S. J. Phytosphingosine in combination with ionizing radiation enhances apoptotic cell death in radiation-resistant cancer cells through ROS-dependent and-independent AIF release. *Blood* **2005**, *105* (4), 1724−33.

(24) Liang, Y.; Huang, W.; Zeng, D.; Huang, X.; Chan, L.; Mei, C.; Feng, P.; Tan, C. H.; Chen, T. Cancer-targeted design of bioresponsive prodrug with enhanced cellular uptake to achieve precise cancer therapy. *Drug Delivery* **2018**, *25* (1), 1350−1361.

(25) Leung, K. Y.; De Castro, S. C.; Savery, D.; Copp, A. J.; Greene, N. D. Nucleotide precursors prevent folic acid-resistant neural tube defects in the mouse. *Brain* **2013**, *136* (9), 2836−41.

(26) Chen, C.; Ke, J.; Zhou, X. E.; Yi, W.; Brunzelle, J. S.; Li, J.; Yong, E. L.; Xu, H. E.; Melcher, K. Structural basis for molecular recognition of folic acid by folate receptors. *Nature* **2013**, *500* (7463), 486−9.

https://dx.doi.org/10.1021/acsmedchemlett.0c00105
ACS Med. Chem. Lett. 2020, 11, 1421−1428